

## From Hit to Lead: *De Novo* Design Based on Virtual Screening Hits of Inhibitors of tRNA-Guanine Transglycosylase, a Putative Target of Shigellosis Therapy

by Ruth Brenk<sup>a</sup>), Hans-Dieter Gerber<sup>a</sup>), Jeffrey D. Kittendorf<sup>b</sup>), George A. Garcia<sup>b</sup>), Klaus Reuter<sup>a</sup>), and Gerhard Klebe<sup>\*a</sup>)

<sup>a</sup>) Institut für Pharmazeutische Chemie, Philipps-Universität Marburg, Marbacher Weg 6, D-35032 Marburg

<sup>b</sup>) Interdepartmental Program in Medicinal Chemistry, College of Pharmacy, University of Michigan, Ann Arbor MI 48109-1065, USA

This paper is dedicated to Professor *Jack D. Dunitz* on the occasion of his 80th anniversary

---

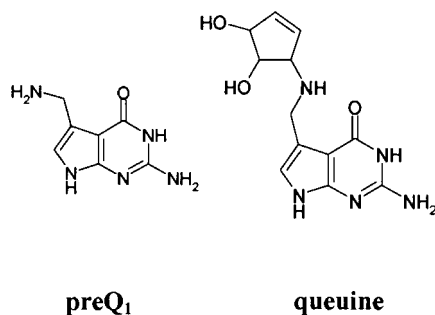
Shigellosis, a bacterial disease, causes the death of more than one million people per year. Extensive studies of *Shigella flexneri* have recognized tRNA-guanine transglycosylase (TGT, EC 2.4.2.29) as one of the key enzymes involved in the regulation of bacterial virulence. Based on the crystal structure of the *Zymomonas mobilis* enzyme, we have embarked on the rational design of TGT inhibitors. Herein, we describe the structure-based optimization of hits previously found by virtual screening (see *Tables 1–3*). For the pteridines, the most potent compound class discovered in a previous virtual screening run, a versatile synthesis could be established giving access to a broad range of substituted derivatives (see *Scheme 5*). The best ligand in this series, **14**, exhibits a  $K_i = 0.45 \mu\text{M}$ .

---

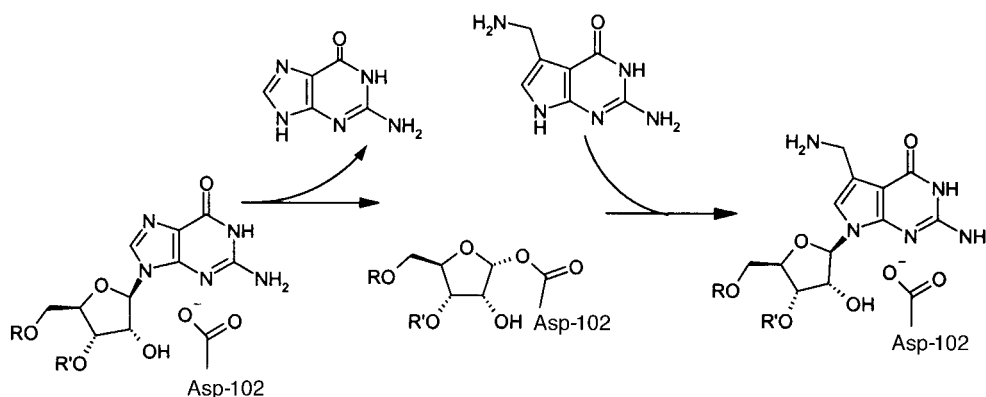
**Introduction.** – Shigellosis, a bacterial disease, causes death of more than one million people per year [1], mainly in the developing countries with substandard hygiene and water supplies. Usually, this disease is treated by antibiotics [2][3], but increasingly multidrug-resistant strains are reported. Accordingly, there is urgent demand for the development of new and selective antibiotics against shigellosis [4].

Extensive studies of *Shigella flexneri* have recognized tRNA-guanine transglycosylase (TGT, EC 2.4.2.29) as one of the key enzymes involved in the regulation of bacterial virulence [5][6]. In eubacteria, it catalyzes the incipient step in biosynthesis of the highly modified nucleoside queuine (see *Fig. 1*), which is inserted in the anticodon loop of certain tRNAs. The exchange of guanine in the unmodified tRNA by the queuine precursor preQ<sub>1</sub> (= 7-(methylamino)-7-deazaguanine; see *Scheme 1*) is performed *via* an associative mechanism [7][8]. Once bound to tRNA, preQ<sub>1</sub> is further chemically modified through at least two subsequent enzymatic steps to result in the final queuine modification [9][10]. The presence of such modified bases in the anticodon loop supposedly modulates the efficiency and fidelity of tRNAs during translation [11–13]. Inhibiting the biological function of TGT is expected to result in tRNAs lacking the modified base in the anticodon. This leads to a significantly reduced expression of the *virF* gene resulting in a dramatic loss of virulence [5][14].

Based on the crystal structure of the *Zymomonas mobilis* enzyme [15], which exhibits an active site of identical composition apart from a Tyr-106 Phe replacement [16], we have embarked on the rational design of TGT inhibitors. In a recent study, we

Fig. 1. Chemical structures of preQ<sub>1</sub> and queuine

Scheme 1. *Catalytic Mechanism of TGT*. TGT catalyzes the base exchange of guanine in the wobble position of certain tRNAs against preQ<sub>1</sub>. The reaction follows an associate mechanism *via* a covalent intermediate.



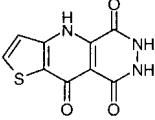
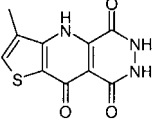
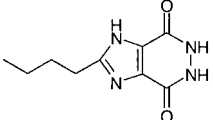
performed a virtual screening [17] applying a protocol of several consecutive hierarchical filters, involving a preselection based on functional-group requirements and fast pharmacophore matching. In a first step, a suitable pharmacophore has been derived applying a sophisticated ‘hot-spot’ analysis of the binding site to detect regions of favorable protein–ligand interactions. After a crude screening for compounds in agreement with this protein-derived pharmacophore, flexible docking of the best candidate molecules was performed. A remarkable variety of structurally deviating hits has been detected by this approach. Experimental testing of the most-promising hits demonstrated several of the test compounds as micromolar to sub-micromolar level inhibitors. In a following step, described in the present paper, these hits have to be validated and assessed whether they are suitable as potential leads for further development and optimization. In this context, the synthetic accessibility and the versatility of the functional decoration for chemical modifications of the discovered hits has to be explored. Furthermore, the chemical modifications planned by rational concepts are used to map different subsites of the binding pocket of TGT. Preliminary structure–activity relationships help to rank the constitutions of different binding subsites to elucidate their relevance to enhance binding affinity. In a recent study [18],

we started with 2-aminoquinazolin-4(3*H*)-one as a promising scaffold of TGT inhibitor design. In an iterative drug-design process involving crystallography, computer design, synthesis, and enzyme testing, we succeeded to establish a first compound class binding to the target enzyme with sub-micromolar affinity. In the present contribution, we report on other compound classes possessing the potential to deliver an additional lead structure for further optimization to result in high-affinity TGT inhibitors.

**Results and Discussion.** – *Dihydro-pyridazino-quinoline-triones.* In a virtual screening run described previously, **1** and **2** (Table 1) have been discovered as low micromolar inhibitors of TGT [17]. Probably due to their limited solubility under aqueous-buffer conditions, we failed to soak these compounds into crystals of uncomplexed TGT. However, soaking was successful for compound **3**, which was detected in the same screening run. Crystal-structure analysis of this compound in complex with TGT (PDB-Code 1N2V) revealed an unexpected flip of a backbone peptide group in the binding pocket (Fig. 2). The backbone carbonyl group of Leu-231, originally exposed towards the binding site in all previously studied complexes, becomes buried, whereas the donor functionality of the adjacent backbone NH is now available for ligand binding. In addition, an interstitial H<sub>2</sub>O molecule is incorporated, thus mediating a favorable protein–ligand interaction. Based on the complex structure with **3**, the binding modes of **1** and **2** could be modeled accordingly (Fig. 2). Therefore, a plausible binding mode can be assumed for **1**, which exhibits binding affinity to TGT in the low micromolar range. Furthermore, a three-step synthesis of this compound has been published [19]. These aspects strongly argue to consider **1** as a prospective lead structure for new TGT inhibitors.

To discover suitable regions in the binding pocket where additional molecular portions and functional groups hooked-up to **1** could possibly interact with the protein to further improve binding affinity, a ‘hot-spot’ analysis (see *Exper. Part*) was performed. The result of such calculations by means of a H-bond-donor probe (N.3) is

Table 1. Three Pyridazinediones Retrieved in the Previous Virtual Screening and Tested for TGT Inhibition

Structure	$K_i$ [ $\mu\text{M}$ ] <sup>a)</sup>	Structure	$K_i$ [ $\mu\text{M}$ ] <sup>a)</sup>
<b>1</b> 	$5.0 \pm 1.2$	<b>3</b> 	$83 \pm 18$
<b>2</b> 	$4.7 \pm 1.0$		

<sup>a)</sup> The error given is the standard deviation of two independent measurements with different substrate concentrations. Due to the elaborate determination of the  $K_i$  values, the actual error is assumed to be ca. 20–30% [34].

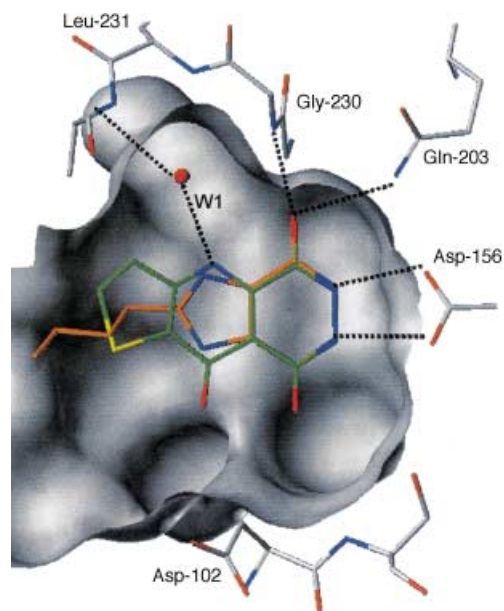


Fig. 2. Superposition of the crystallographically determined binding mode of **3** (orange) with the modeled binding mode of **1** (green). Both ligands can form a H-bond to the interstitial H<sub>2</sub>O molecule W1.

shown in *Fig. 3*. The three N-atoms of **1** fall precisely into regions where the analysis predicts favorable areas. Additionally, two so far unused ‘hot-spot’ areas are found near Asp-102 and Asp-280. The first design goal was, therefore, to decorate **1** accordingly with further functional groups to address these additional regions and to hopefully gain in affinity. Considering in detail the required topological connectivity, the core structure of **1** does not appear ideally suited for this optimization due to the placement of the S-atom in the thiophene moiety. For chemical reason, no further portions can be linked *via* the S-atom. Focusing on the 2-position as substitution site appears rather unreasonable due to steric reasons since substituents at this position could rather unlikely address the indicated ‘hot spots’ but would orient towards the rim of the binding pocket. Therefore, in the first step, the thiophene ring of **1** was replaced bioisosterically by a benzene ring (*Scheme 2*). Within the error limits of the biochemical assay, the affinity of **4** ( $3.7 \pm 1.5 \mu\text{M}$ ) remained unchanged compared to **1** ( $5.0 \pm 1.2 \mu\text{M}$ ). For subsequent decoration of **4**, positions 8 and 9 appear suitable. For this purpose, an OH group was introduced into the new core structure that could serve as a linker at C(8). A versatile synthesis concept for this compound class starts with substituted anthranilic acid (*Scheme 3*). In a first trial, we selected the 2-amino-5-hydroxy derivative (R=OH). After esterification and addition to the triple bond of but-2-ynedioic acid ester, the central pyridinone ring was closed. The dihydropyridazine ring moiety was introduced by means of hydrazine. Due to synthetic reasons, any substituent at the linker OH group had to be introduced into the hydroxyanthranilic acid prior to the construction of the central ring moiety.

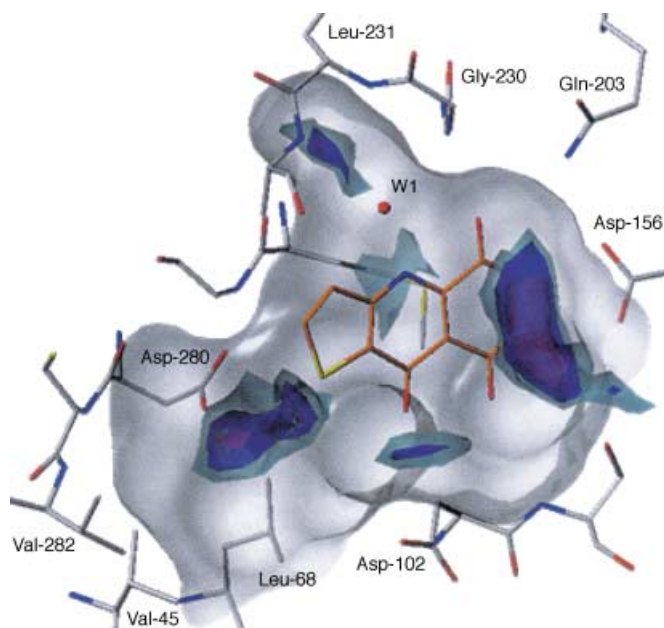
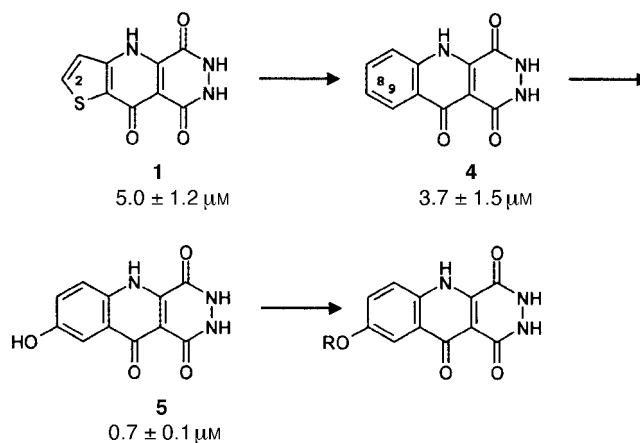


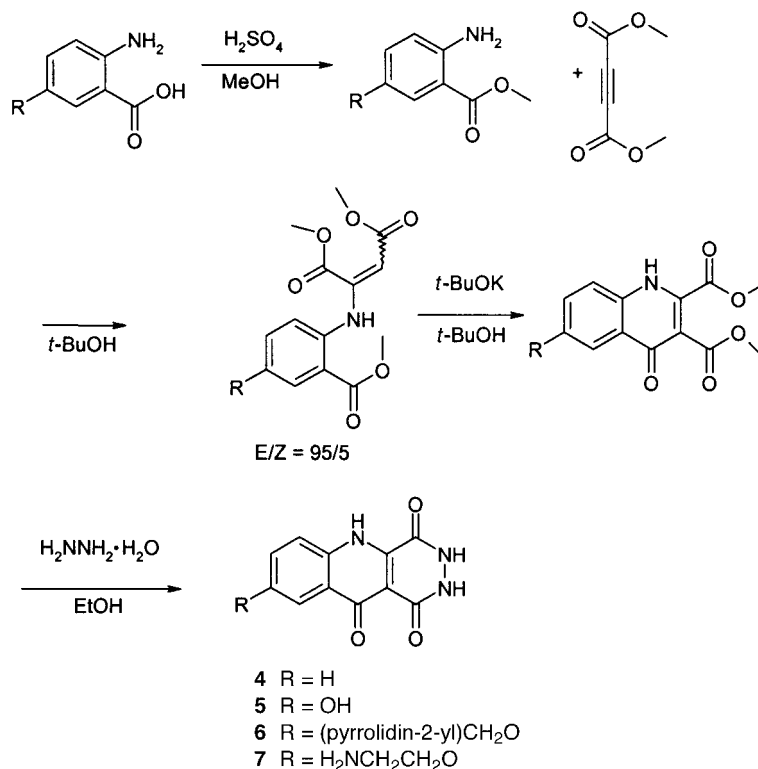
Fig. 3. Mapping of putative 'hot spots' of binding in the active site of TGT for an *N.3* probe. The 'hot spots', calculated with DrugScore, are contoured at a 80 (cyan), 84 (blue), and 88% (magenta) level above the global minimum. For orientation, the modeled-binding geometry of **1** is also shown.

Scheme 2. Optimization of **1** via Bioisosteric Replacement. The  $K_i$  values are given.



Already, the introduction of the OH group at C(8) improved binding affinity leading to a  $K_i$  value of  $0.7 \mu\text{M}$  for **5**. Molecular modeling based on MOLOC [20] and SYBYL [21] suggested that a  $\text{CH}_2\text{CH}_2\text{NH}$  chain added to **5** could successfully address the 'hot spot' near Asp-280. Directly in the neighborhood of this polar spot, a small hydrophobic pocket opens, formed by the amino acids Val-45, Leu-68, Cys-281, and

Scheme 3. General Synthesis Scheme for Dihydro-pyridazino-quinoline-triones 4–7



Val-282. The ‘hot-spot’ analysis based on a C.3 probe indicates favorable binding of hydrophobic groups in this area (Fig. 4,b).

In a previous study, we successfully addressed this pocket during the optimization of quinazolinone derivatives as TGT inhibitors [18]. In consequence, we tried to design a compound that could occupy both the hydrophobic pocket and the donor spot near Asp-280. A pyrrolidine moiety appeared to be a suitable candidate. The modeled binding mode of **6** (Table 2) is shown in Fig. 4. In the computed binding mode, the aliphatic C-atoms of the pyrrolidine ring fill the hydrophobic pocket (Fig. 4,b), and its N-atom donates a H-bond to Asp-280 (Fig. 4,a). The pK<sub>a</sub> of pyrrolidine in H<sub>2</sub>O is reported to be 11.35 [22]. We, therefore, assume that this group is positively charged in the binding pocket leading to a charge-assisted H-bond with Asp-280. Depending on the local surrounding of such H-bonds, an affinity increase of up to 3000-fold could be expected compared to the unsubstituted derivative [23–25]. Furthermore, all torsion angles of **6** in its bound conformation are indicated as energetically favorable [26]. To our surprise, the K<sub>i</sub> value of **6** did not improve compared to the unsubstituted parent structure. Indeed, a K<sub>i</sub> of 9.4 μM indicates even reduced binding compared to the core structure **4**. To investigate whether the aliphatic C-atoms of the pyrrolidine moiety are responsible for this effect, we considered testing the structurally reduced analogue **7**

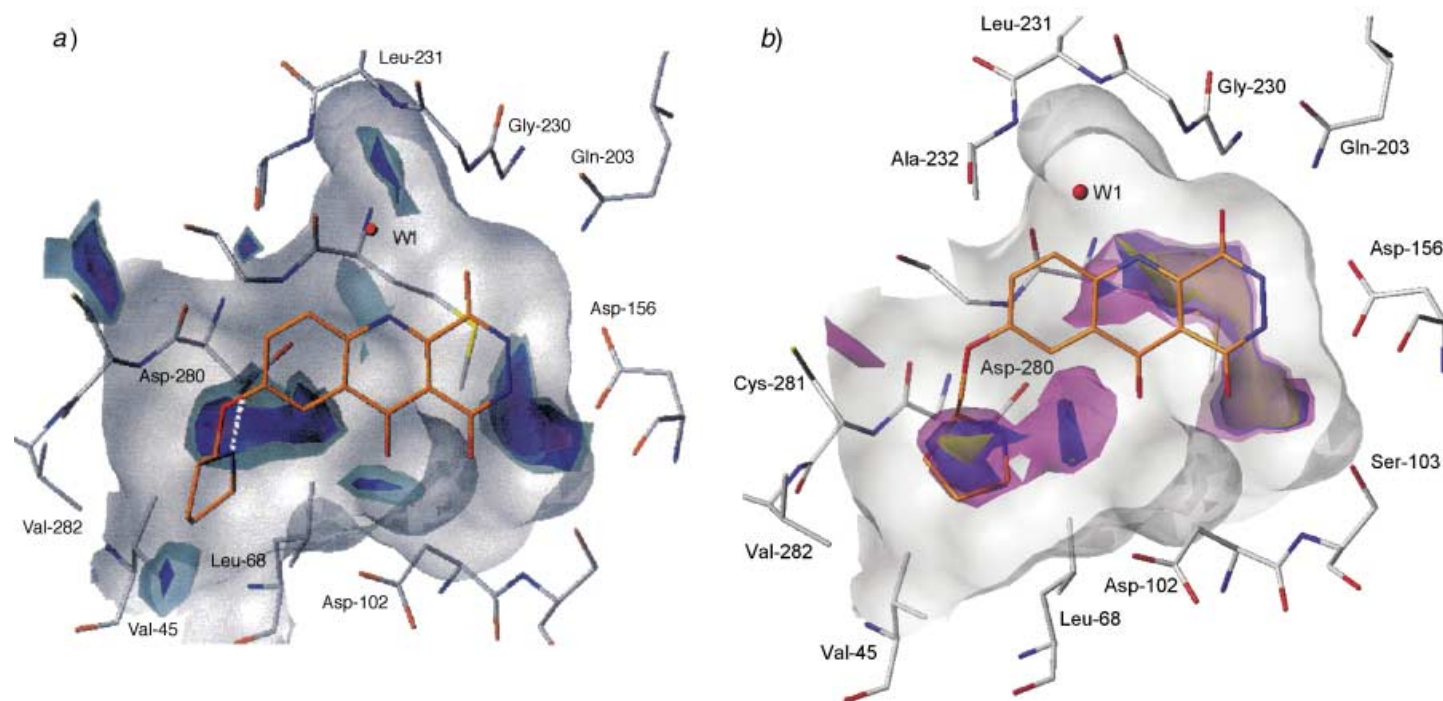
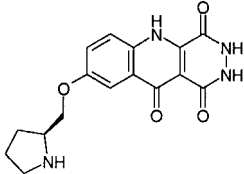
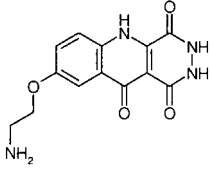
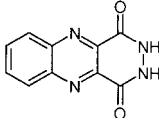


Fig. 4. *Modeled binding mode of 6*: a) 'Hot spots', calculated with DrugScore for an *N.3* probe contoured at a 80 (cyan), 84 (blue), and 88% (magenta) level above the global minimum; all H-bond donors of the ligand fall into regions where their presence is predicted to be favorable; the N-atom of the pyrrolidine ring forms a H-bond to Asp-280). b) 'Hot spots', calculated with DrugScore for a *C.3* probe contoured at a 88 (magenta), 90 (blue), and 92% (yellow) level; the aliphatic C-atoms of the pyrrolidine ring fill the hydrophobic pocket formed by Val-45, Leu-68, Cys-281, and Val-282).

Table 2. Dihydro-pyridazino-quinoline-triones and a Dihydro-tetraaza-anthracenedione Synthesized and Subsequently Tested for TGT Inhibition

Structure	$K_i$ [ $\mu\text{M}$ ] <sup>a)</sup>	Structure	$K_i$ [ $\mu\text{M}$ ] <sup>a)</sup>
	$9.4 \pm 0.1$		$5.6 \pm 0.4$
	–		

<sup>a)</sup> The error given is the standard deviation of two independent measurements with different substrate concentrations. Due to the elaborate determination of the  $K_i$  values, the actual error is assumed to be ca. 20–30% [34].

lacking these C-atoms. However, compound **7** polymerized, probably, because its terminal amino group reacts with the carbonyl group of the pyridinone ring. Unfortunately, it could not be tested for biological activity.

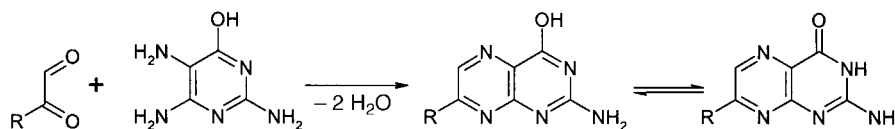
Analyzing in detail the suggested binding mode of **1** and its dihydro-pyridazino-quinoline-trione analogues **4–7** (Figs. 3 and 4), the above-mentioned possibly reactive carbonyl group is not involved in any favorable interactions with the surrounding amino acids. As a consequence, it should be possible to avoid this for the stability of the compound class unfortunate functional group without losing affinity. Accordingly, we considered dihydro-tetraaza-anthracenes (= dihydro-pyridazino-quinoxalines) such as **8** as possible bioisosteric analogues of **4**. In comparison to **4**, the pyridinone ring is replaced by a pyrazine ring in **8**. This exchange corresponds to the replacement of a H-bond donor facility of the pyridinone by a H-bond acceptor in the pyrazine ring. The inhibitor presumably interacts *via* this functional group with the interstitial H<sub>2</sub>O molecule W1. However, due to its bifunctionality, this H<sub>2</sub>O molecule can act either as a H-bond donor or acceptor with respect to the ligand functional group [17]. Therefore, it can be expected that this exchange does not affect binding affinity. This new compound class of dihydro-tetraaza-anthracene-diones is synthetically accessible *via* a route described by *Chattaway and Humphrey* [27]. Interestingly, the  $K_i$  value of **8** is 5.6  $\mu\text{M}$ , and falls indeed into the same range as that of **4**. Unfortunately, the yield of the followed synthetic route is very low; thus, **8** does not appear to be a suitable choice for a prospective lead structure.

*Pteridines.* For both compound classes, dihydro-pyridazino-quinoline-triones and dihydro-tetraaza-anthracene-diones described above, unexpected difficulties occurred during synthesis. This prompted us to search for a better-suited lead structure that could be more easily modified. In a virtual screening run, we discovered pteridines to be



potent inhibitors of *Z. mobilis* TGT. Experimental verification of this suggested hit demonstrated 2-aminopteridin-4(3*H*)-one to be a 0.6  $\mu\text{M}$  inhibitor [17]. This compound is synthetically accessible in a one-step reaction starting from 2,4,5-triaminopyrimidin-6-ol and glyoxal (= ethanedial; *Scheme 4*) [28]. If instead of glyoxal (R=H) substituted keto aldehydes are used, pteridines substituted at the 6- or 7-position are obtained [29]. Obviously, pteridines are a well-studied class of compounds, readily derivatized: more than 60 2-aminopteridin-4(3*H*)-ones with varying substituents at the 7-position are stored in the *Beilstein Database* (status October 2002). This makes 2-aminopteridin-4(3*H*)-one an interesting suggestion as a lead structure for TGT inhibitors.

Scheme 4. General Synthesis Scheme for 2-Aminopteridin-4(3*H*)-ones



Presumably, 2-aminopteridin-4(3*H*)-one adopts a similar binding mode as **3**. The modeled binding geometry is shown in *Fig. 5*. In this orientation, it places its H-bond donors in regions indicated as favorable in the ‘hot-spot’ analysis. However, again, it leaves the ‘hot spot’ near Asp-280 as well as the hydrophobic pocket formed by Val-45, Leu-68, Cys-281, and Val-282 unoccupied. Accordingly, we decided to address these areas of the binding pocket by substituents attached to C(7) of the pteridine skeleton.

Simple access to pteridines follows the reaction of substituted aldehydes with 2,4,5-triaminopyrimidinol (*Scheme 4*). Starting with substituted ketoaldehydes, constitutional isomers have to be expected. To yield the desired isomer, the reaction conditions have to be optimized for each starting material individually. They depend on the ketoaldehyde used and must be re-established for any new reagent. To circumvent this obvious disadvantage, we selected a pteridine derivative as core structure that already incorporated an appropriate substituent at C(7) as precursor for a linker functional group. After functionalizing this linker, differently substituted compounds could be obtained avoiding possible constitutional isomers.

A pteridine with suitable precursor for a potential linker group is 2-amino-7-methylpteridin-4(3*H*)-one (**9**; *Table 3*); the Me group can be easily functionalized by bromination. Subsequently, the Br-atom can be substituted by different S- and O-nucleophiles to introduce suitable side chains. For all respective steps, related syntheses have been described in the literature [29–31], the best yield for the last step of the reaction being obtained for S-nucleophiles [31]. Following the three subsequent reaction steps shown in *Scheme 5*, different pteridine derivatives should be easily available. According to the expected yield in the first design cycle, only S-nucleophiles were considered.

To select appropriate thiols, the *Available Chemicals Directory (ACD)* was screened as an idea generator following a hierarchical protocol. First, the database was screened with SELECTOR [32] for aliphatic thiols. Out of 215212 compounds, only 701 passed this criterion. In a next step, the remaining hitlist was filtered for compounds that contained exactly one thiol group along with a molecular mass of less than 300 D and up to six rotatable bonds. These criteria were chosen to reveal unique

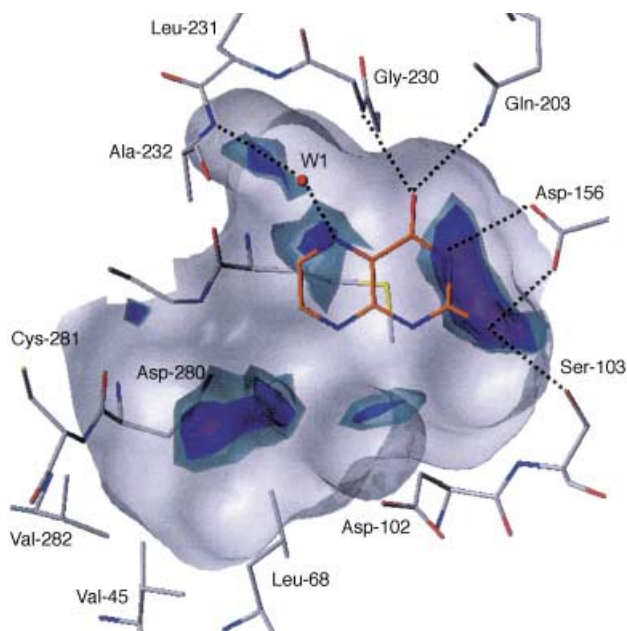


Fig. 5. Modeled binding mode of 2-aminopteridin-4(3H)-one together with 'hot spots', calculated with DrugScore for an N.3 probe. 'Hot spots' contoured at a 80 (cyan), 84 (blue), and 88% (magenta) level. The ligand can form a H-bond to the interstitial H<sub>2</sub>O molecule W1. The unoccupied 'hot spot' near Asp-280 as well as the hydrophobic pocket formed by Val-45, Leu-68, Cys-281, and Val-282 can be addressed via substitutions at C(7).

product formation during synthesis and to avoid compounds with high molecular mass and pronounced flexibility. After this step, 204 compounds remained. Filtering the hitlist for duplicates reduced the number of prospective candidates to 148 compounds.

Scheme 5. Synthesis of Derivates of 2-Aminopteridin-4(3H)-ones with Substituents at C(7)

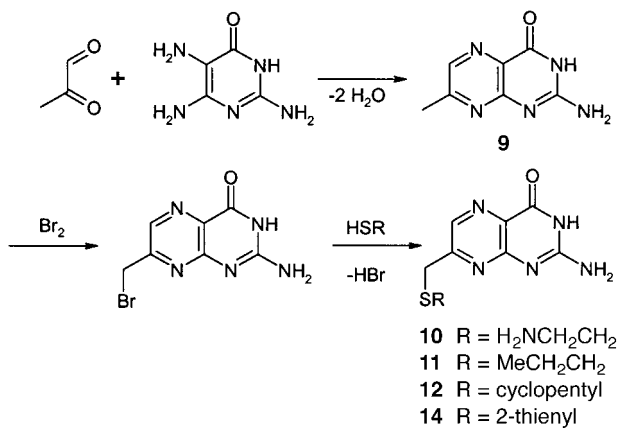
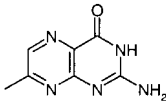
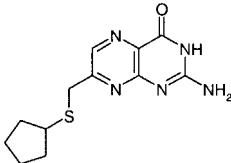
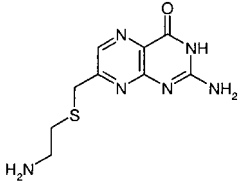
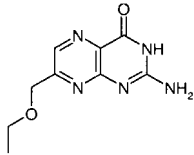
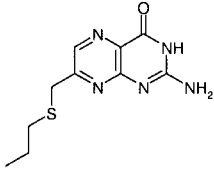
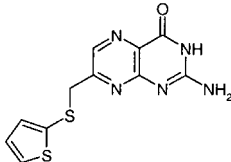


Table 3. Pteridinones that were Synthesized and Subsequently Tested for TGT Inhibition

Structure	$K_i$ [ $\mu\text{M}$ ] <sup>a)</sup>	Structure	$K_i$ [ $\mu\text{M}$ ] <sup>a)</sup>
	$5.6 \pm 1.7$		$5.2 \pm 0.8$
	$3.4 \pm 0.4$		$6.7 \pm 0.9$
	$7.9 \pm 1.9$		$0.45 \pm 0.05$

<sup>a)</sup> The error given is the standard deviation of two independent measurements with different substrate concentrations. Due to the elaborate determination of the  $K_i$  values, the actual error is assumed to be ca. 20–30% [34].

By using a SPL script in SYBYL [21], these fragments were assembled to putative pteridine-type inhibitors. Subsequently, they were docked with FlexX [33] into the binding pocket of the *Z. mobilis* TGT. For 144 of the candidate molecules, a docking solution was generated. Subsequently, the obtained hitlist was inspected visually. Prospective-looking hits were minimized by using the MAB force field [20] simultaneously keeping the binding pocket rigid. A final selection for synthesis and enzyme testing regarded in particular the following criteria: *a)* synthetic accessibility, *b)* complementarity between ligand and protein surface in terms of spatial occupancy and matching contacts in hydrophobic/hydrophilic surface patches, *c)* absence of unfavorable *Van der Waals* interactions after minimization, and *d)* diversity of the attached fragments within the considered series. The compounds **10–12** finally selected are shown in Table 3. Compound **13** was obtained as an O-analog and tested for comparison. Derivative **12** with a terminal cyclopentyl moiety was expected to occupy the small hydrophobic binding niche composed by Val-45, Leu-68, Cys-281, and Val-282. Since the ‘hot-spot’ analysis (see below, Fig. 8) indicated favorable binding of hydrophobic moieties to this subsite, the analogous derivative **14** with a terminal thiophene group was selected likewise.

Surprisingly, the  $K_i$  value of 2-amino-7-methylpteridin-4(3H)-one (**9**) is by about one order of magnitude higher than that of the parent pteridine (5.6 vs. 0.6  $\mu\text{M}$ ). Consulting force-field calculations with MOLOC did not reveal any unfavorable interactions for the Me group of **9** with the protein environment. Thus, a simple

explanation for this finding cannot be provided. Possibly, the additional Me group ruptures a H-bond network mediated by interstitial H<sub>2</sub>O molecules to polar residues in the binding pocket. Such interactions have been observed in the crystal structures of 3,5-diaminophthalhydrazide with the enzyme [34].

The best docking solution of **10** suggested by FlexX is shown in Fig. 6. According to this binding geometry, the terminal NH<sub>2</sub> group forms a H-bond to Asp-280. Due to chemical reasons, a similar H-bond cannot be established by **11** and **12**. Nevertheless, the *K<sub>i</sub>* values of all three compounds fall, within the error limits of the assay, into the same range as the lead compound **9** (*K<sub>i</sub>* = 5.6 (**9**), 3.4 (**10**), 7.9 (**11**), 5.2 (**12**) μM). Obviously, and in agreement with the results described for the pyridazinedione series, the assumed charge-assisted H-bond, likely to be formed by **10**, cannot improve affinity significantly compared to **9**. Furthermore, the purely lipophilic moieties of **11** and **12** do not improve binding affinity either.

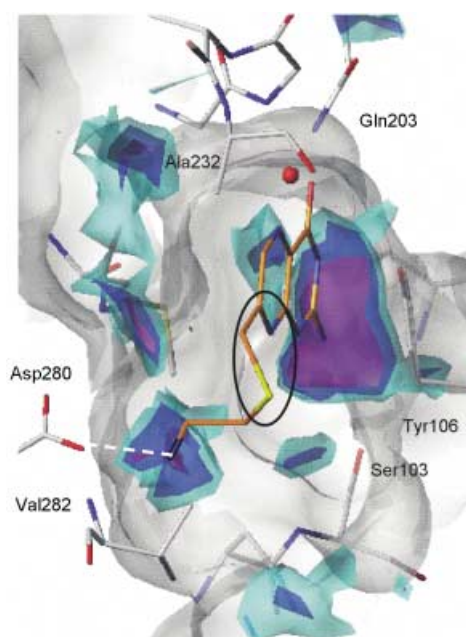


Fig. 6. Best-ranked docking solution for **10** together with 'hot spots', calculated with DrugScore for an N.3 probe, 'Hot spots' contoured at a 80 (cyan), 84 (blue), and 88% (magenta) level. In the suggested binding mode, the terminal NH<sub>2</sub> group forms a H-bond to Asp-280. The conformational angle N(arom.)–C(arom.)–C(sp<sup>3</sup>)–S(sp<sup>3</sup>) (circle) adopts a value of ca. 30° which does not correspond to the most favorable arrangement of this torsional fragment.

Consulting conformational preferences as observed in small-molecule crystal structures (see, e.g., the MIMUMBA approach [26]), energetically favorable conformers of the torsional fragment N(arom.)–C(arom.)–C(sp<sup>3</sup>)–S(sp<sup>3</sup>) (Fig. 7) correspond to values of 0°, 90°, and 180°. The conformer at 90° is the most favorable conformation followed by the arrangement at 0°. But the first conformation cannot be adopted by the pteridine derivatives **10**–**12** at the binding site due to unfavorable steric

interactions with Tyr-106 and Gly-261 on either sides of the binding pocket. All derivatives could be accommodated with the less-favorable value of  $0^\circ$  for this torsional fragment. However, if this angle is adopted by **10**, the assumed H-bond to Asp-280 could not be formed. To achieve this interaction, the torsion angle must be shifted to *ca.*  $30^\circ$ , thus driving this fragment significantly out of a local minimum. Possibly, this slightly unfavorable arrangement could be one explanation for why the assumed charge-assisted H-bond to Asp-280 does not increase binding affinity. Furthermore, there are indications from enzyme kinetics that Asp-280 acts as a general acid/base during the enzyme reaction (*Scheme 1*) [35]. In such a case, its functional role would be to protonate the leaving guanine moiety and to deprotonate the incoming preQ<sub>1</sub>. As a consequence, Asp-280 would be protonated most of the time. Accordingly, its pK<sub>a</sub> value is expected to exhibit a higher value than measured for the free acid. Therefore, much less-favorable H-bond-acceptor properties are expected for Asp-280. This assumption is supported by our observation that the placement of positively charged donor groups (*e.g.*, in **6** or **10**) in the neighborhood of Asp-280 does not improve binding affinity. Nevertheless, it also has to be kept in mind that the enzymatic reaction used to record inhibition data involves tRNA binding to TGT. Thus, possibly through tRNA complexation, the conformation and local properties of Asp-280 could be affected.

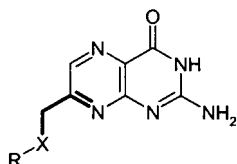


Fig. 7. Torsion Angle  $N(\text{arom.})-C(\text{arom.})-C(\text{sp}^3)-X$  ( $X=S(\text{sp}^3)$ ,  $O(\text{sp}^3)$ ). Favorable angles for  $X=S$  are  $0^\circ$ ,  $90^\circ$ , and  $180^\circ$  with the arrangement at  $90^\circ$  as most favorable. For  $X=O$ , conformers at  $0^\circ$ ,  $90^\circ$ , and  $180^\circ$  are energetically well disposed, the arrangement at  $0^\circ$  is most preferred, with a broad distribution around the maxima. These considerations are based on statistical preferences observed in torsional libraries retrieved from small-molecule crystal structures [26].

The ethoxy derivative **13** shows a  $K_i$  of  $6.7 \mu\text{M}$ . It falls into the same range as the unsubstituted lead **9**. In directly comparing its properties to those of **11**, it has to be considered that the side chain of the latter is extended by one  $\text{CH}_2$  group. Cases have been reported where an optimally placed additional Me group increases binding affinity by a factor of 10 [23–25]. Nevertheless, it seems likely in the present case that the substitution of S for O has no dramatic influence on affinity. The conformational preferences of an  $N(\text{arom.})-C(\text{arom.})-C(\text{sp}^3)-O(\text{sp}^3)$  fragment differ from those of the previously described  $N(\text{arom.})-C(\text{arom.})-C(\text{sp}^3)-S(\text{sp}^3)$  chain (*Fig. 7*). In the O-case, favorable angles are  $0^\circ$ ,  $90^\circ$ , and  $180^\circ$ , and the  $0^\circ$  conformer corresponds to the global minimum. Furthermore, a C–O bond length is by  $0.4 \text{ \AA}$  shorter than a C–S bond. Therefore, 7-(oxymethyl)pteridines such as **13**, in contrast to 7-(thiomethyl)pteridines, can adopt a torsion angle of  $90^\circ$  in the binding pocket of TGT without creating steric conflicts with the surrounding amino acids. Additionally, the distribution of torsion angles around  $90^\circ$  is quite broad, thus, slight distortions to lower values appear energetically equivalent. Accordingly, 7-(oxymethyl)pteridines possibly exhibit better-suited conformational properties compared to the 7-(thiomethyl)pteridines to properly accommodate the binding pocket. Moreover, data for a large variety of alcohols are stored in the *ACD*. In a subsequent design cycle, we want to investigate

whether such derivatives can further improve the affinity of the lead structure by using such side chains.

The most-potent inhibitor in the discussed series is **14**. With  $0.45\ \mu\text{M}$ , its  $K_i$  value is more than one order of magnitude lower compared to the original lead structure **9**. The modeled binding mode is shown in *Fig. 8* together with ‘hot spots’ calculated with DrugScore using a C.ar probe. The thiophene ring fully accommodates the binding niche formed by Val-45, Leu-68, Cys-281, and Val-282. This area is predicted to be favorable for aromatic C-atoms. In a following design cycle, we will further map the molecular-recognition properties exhibited by this subpocket using other aromatic portions. Interestingly, in a previous optimization study based on quinazolinones as the core skeleton, we also found that an aromatic moiety ideally fits into this hydrophobic binding niche simultaneously increasing the binding affinity [18].

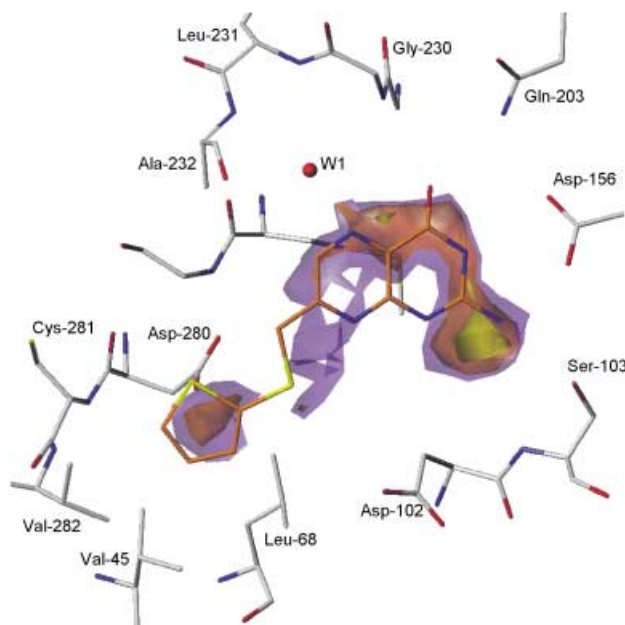


Fig. 8. Modeled binding mode of **14** together with ‘hot spots’, calculated with DrugScore for a C.ar-probe. ‘Hot spots’ contoured at a 89 (purple), 91 (orange), and 95% (yellow) level. The thiophene moiety falls exactly into a region predicted as favorable for aromatic C-atoms.

**Conclusions.** – Starting with various hits from virtual screening, we tried to improve binding affinity focusing mainly on two lead structures. Two compound classes, the dihydropyridazino-quinoline-triones and dihydro-tetraaza-anthracene-diones, resulted in unexpected problems during synthesis. For the pteridines, the most-potent compound class discovered in a previous virtual screening run, a versatile synthesis could be established giving access to a broad range of substituted derivatives. Based on structural information present in the *ACD* and guided by the results of ‘hot-spot’ analyses, several new inhibitors were synthesized and tested. The best ligand, **14**, in this

series exhibits a  $K_i = 0.45 \mu\text{M}$ . The thiophene moiety of this compound accommodates exactly a region in the binding pocket that is predicted to be favorable for aromatic C-atoms. In a following design cycle, we will try to further experience the molecular-recognition properties exhibited by this subpocket using different aromatic portions.

### Experimental Part

1. *Molecular Modeling*. The modeling was performed with SYBYL 6.8 [21] and MAB/Moloc 01/05/08 [20] running on a *Silicon-Graphics-O2* (R10000) workstation.

2. *'Hot-Spot' Analysis of the Binding Pocket*. 'Hot spots' were calculated with DrugScore [36] by using the unoccupied binding pocket of TGT in its conformation adopted with the bound ligand **3** (PDP-code 1N2V). In these calculations, the position of the interstitial H<sub>2</sub>O molecule W1, assigned to atom-type O.3, was considered. The N.3 probe was selected to analyze H-bond-donor interactions, and the C.ar probe as well as the C.3 probe were used to map hydrophobic interactions. 'Hot spots' are contoured on percentage levels with respect to the global minimum.

3. *Construction of 3D Database*. The 2D connection tables of entries in the *Available Chemicals Directory* (ACD) were converted as described in [17].

4. *Hierarchical Filtering*. The hierarchical filtering was performed by using SELECTOR [32]. The SLN code (Sybyl line notation) for the required aliphatic thiol fragments was defined as SHCH2.

5. *Docking*. With an in-house script, exocyclic guanidino and amidino groups or primary and secondary aliphatic amino groups were protonated; similarly, phosphoric, sulfonic, and carboxylic acid groups were deprotonated. Docking calculations were performed with FlexX, version 1.102. To speed up calculations, the 'mapref' mode was activated, and all pteridines were matched on a preoriented core structure. The FlexX scoring function was used during the complex-construction phase. The obtained solutions were reranked by DrugScore [37] as implemented into FlexX.

6. *Force-Field Minimization*. Ligands were minimized in the binding pocket exhibiting the protein conformation as complexed with **3** by using the MAB force field [20]. The default parameters were applied, and the binding pocket was kept rigid.

7. *Kinetic Analysis*. The apparent  $K_i$  values were measured as described elsewhere [34].

8. *Syntheses*. 8.1. *General*. Starting compounds were purchased from *Sigma-Aldrich Chemie GmbH*. Unless stated otherwise, commercially available solvents were used without further purification. Column chromatography (CC): silica gel 60 (0.063–0.200 mm), *Merck*, solvents for CC were distilled before use. NMR Spectra: *Jeol JNM-GX 400* (<sup>1</sup>H at 399.79 MHz, '400 MHz'; <sup>13</sup>C at 100.54 MHz, '100.5 MHz') or *Jeol Lambda 500 Delta* (<sup>1</sup>H at 500.00 MHz, '500 MHz'; <sup>13</sup>C at 125.65 MHz, '125.7 MHz');  $\delta$  in ppm referenced to SiMe<sub>4</sub> (= 0.00 ppm) for <sup>1</sup>H and to CDCl<sub>3</sub> (= 77.00 ppm) or DMSO (= 39.50 ppm) for <sup>13</sup>C,  $J$  in Hz; due to poor solubility, only <sup>1</sup>H-NMR spectra were obtained for all pteridine compounds, recorded in 20% DCl/D<sub>2</sub>O (referenced to 5.48 ppm); <sup>13</sup>C-NMR assignments are in some cases subject to change. MS: double-focussing sectorfield mass spectrometer *VG 7070 H* by *Vacuum Generators* or *VG-AutoSpec* by *Micromass* applying electron impact (EI) ionization, in  $m/z$  (rel. %).

8.2. *Dihydro-thieno-pyrido-pyridazine-trione 1 and Dihydro-pyridazino-quinoline-triones 4–6*. 6,7-Dihydrothieno[2,3':5,6]pyrido[2,3-d]pyridazine-5,8,9(4H)-trione (**1**) was prepared according to [19].

2,3-Dihydropyridazino[4,5-b]quinoline-1,4,10(5H)-trione (**4**). Analogously to the three-step synthesis of **1**, from methyl 2-aminobenzoate (5.0 mmol) (see also [38]): 0.75 g (66%) of **4**. Light-yellow solid. <sup>1</sup>H-NMR (400 MHz, (D<sub>6</sub>)DMSO): 13.14, 12.51, 12.31 (3s, 3 NH); 8.29 (*d*, <sup>3</sup> $J$  = 8.1, H–C(9)); 8.16 (*d*, <sup>3</sup> $J$  = 8.2, H–C(6)); 7.93 (*dd*, <sup>3</sup> $J$  = 7.8, 7.2, H–C(8)); 7.57 (*dd*, <sup>3</sup> $J$  = 7.8, 7.5, H–C(7)). <sup>13</sup>C-NMR (100.5 MHz, (D<sub>6</sub>)DMSO): 178.70 (C(10)); 154.01, 152.46 (C(1), C(4)); 139.67, 137.86 (C(4a), C(5a)); 134.08 (C(9)); 124.59, 124.36 (C(7), C(8)); 123.59 (C(9a)); 119.68 (C(6)); 104.74 (C(10a)). EI-MS: 229 (100,  $M^+$ , C<sub>11</sub>H<sub>7</sub>N<sub>3</sub>O<sub>3</sub><sup>+</sup>).

2,3-Dihydro-8-hydroxypyridazino[4,5-b]quinoline-1,4,19(5H)-trione (**5**). Analogously to the three-step synthesis of **4**, from methyl 5-hydroxy-2-aminobenzoate (1.6 mmol). The latter was obtained by the following procedure: To a soln. of 5-hydroxy-2-aminobenzoic acid (6.13 g, 40.0 mmoles) in MeOH (60 ml), conc. H<sub>2</sub>SO<sub>4</sub> soln. (10 ml) was added cautiously. The mixture was refluxed for 20 h and the major excess of MeOH evaporated. The residual dark suspension was poured into ice, the mixture adjusted to pH 8 with NaHCO<sub>3</sub> soln., and the resulting precipitate filtered. After washing with H<sub>2</sub>O, the product was dried *in vacuo*: methyl ester (5.60 g, 84%). Grey solid, which was recrystallized from EtOH for further purification. <sup>1</sup>H-NMR (400 MHz,

(D<sub>6</sub>)acetone): 7.64 (s, OH); 7.27 (d, <sup>4</sup>J = 2.9, H–C(6)); 6.88 (dd, <sup>3</sup>J = 8.8, <sup>4</sup>J = 2.9 Hz, H–C(4)); 6.70 (d, <sup>3</sup>J = 8.8, H–C(3)); 5.93 (br. s, 2 NH<sub>2</sub>); 3.81 (s, MeO).

*Data of 5*: 320 mg (80%). Brownish solid. <sup>1</sup>H-NMR (500 MHz, (D<sub>6</sub>)DMSO): 8.30 (br. s, OH, 3 NH); 7.82 (d, <sup>3</sup>J = 8.8, H–C(6)); 7.51 (d, <sup>4</sup>J = 2.7, H–C(9)); 7.27 (dd, <sup>3</sup>J = 9.0, <sup>4</sup>J = 2.8, H–C(7)). <sup>13</sup>C-NMR (125.7 MHz, (D<sub>6</sub>)DMSO): 175.60 (C(10)); 159.07, 156.59, 154.00 (C(1), C(4), C(8)); 142.23, 141.84 (C(5a), C(4a)); 128.26 (C(9a)); 126.46, 123.78 (C(6), C(9)); 106.08, 104.55 (C(7), C(10a)). EI-MS: 245 (100, M<sup>+</sup>, C<sub>11</sub>H<sub>7</sub>N<sub>2</sub>O<sub>4</sub><sup>+</sup>).

*2,3-Dihydro-8-[[ (2S)-pyrrolidin-2-yl]methoxy]-pyridazino[4,5-b]quinoline-1,4,10(5H)-trione (6)*. Analogously to the three-step synthesis of **4** and **5** via the following isolated and characterized intermediates *A–D*.

*Methyl 2-Amino-5-[[ (2S)-1-[(tert-butoxycarbonyl]pyrrolidin-2-yl)methoxy]benzoate (A)*. To a soln. of the sodium salt of methyl 2-amino-5-hydroxybenzoate, freshly prepared from methyl 2-amino-5-hydroxybenzoate (1.00 g, 6.0 mmol) and 60% NaH (0.250 g, 6.25 mmol) in anh. DMSO (15 ml), *tert*-butyl (2S)-2-[[ (4-methylphenyl)sulfonyl]oxy]methylpyrrolidine-1-carboxylate (1.78 g, 5.0 mmol); prepared from *tert*-butyl (2S)-2-(hydroxymethyl)pyrrolidine-1-carboxylate according to [39] prior to use, in anh. DMSO (10 ml) was added dropwise, and the mixture was stirred for 1 h. Stirring was continued for another 18 h at 75°. The mixture was poured into H<sub>2</sub>O (100 ml), and after addition of brine (100 ml), it was extracted thoroughly with AcOEt. The combined org. extract was washed with NaOH soln. and then with NaH<sub>2</sub>PO<sub>4</sub> soln., dried (Na<sub>2</sub>SO<sub>4</sub>), and evaporated and the obtained dark-red oil (1.50 g) submitted to CC (silica gel, hexane/AcOEt 3:1): *A* (1.33 g, 63%). Light-yellow oil. <sup>1</sup>H-NMR (500 MHz, CDCl<sub>3</sub>): 7.37 (br. d, H–C(6)); 6.96 (d, H–C(4)); 6.62 (d, H–C(3)); 5.40 (br. s, NH<sub>2</sub>); 4.10–3.30 (*m*, 5 H, CH<sub>2</sub>O, pyr.). 3.87 (s, MeO); 2.10–1.80 (*m*, 4 H, pyr.); 1.46 (s, *t*-Bu).

*Dimethyl (2E)/(2Z)-2-[[4-[[ (2S)-1-[(tert-butoxycarbonyl]pyrrolidin-2-yl)methoxy]-2-(methoxycarbonyl)phenyl]amino]but-2-enedioate (B)*. From *A* (5.0 mmol): *B* (2.17 g, 86%), (*E*)/(*Z*) 95:5 (by <sup>1</sup>H-NMR), after CC (hexane/AcOEt 2:1). Colorless oil. <sup>1</sup>H-NMR (500 MHz, CDCl<sub>3</sub>; (*E*)-isomer): 11.21 (s, NH); 7.48 (br. d, H–C(3')); 6.98 (br. s, H–C(5')); 6.62 (d, H–C(6')); 5.48 (br. s, H–C(3)); 4.20–3.30 (*m*, 5 H, CH<sub>2</sub>O, pyr.); 3.95, 3.78, 3.72 (3s, 3 MeO); 2.05–1.85 (*m*, 4 H, pyr.); 1.47 (s, *t*-Bu). EI-MS: 492 (38, M<sup>+</sup>, C<sub>24</sub>H<sub>22</sub>N<sub>2</sub>O<sub>8</sub><sup>+</sup>).

*Dimethyl 6-[[ (2S)-1-[(tert-butoxycarbonyl]pyrrolidin-2-yl)methoxy]-1,4-dihydro-4-oxo-quinoline-2,3-dicarboxylate (C)*. From *B* (4.4 mmol): *C* (1.31 g, 65%), after CC (hexane/AcOEt 1:3). Light-yellow solid. <sup>1</sup>H-NMR (500 MHz, CDCl<sub>3</sub>): 12.41 (br. d, NH); 7.95 (br. s, H–C(8)); 7.60 (*t'*, H–C(5)); 7.47 (dd, <sup>3</sup>J = 9.2, 2.7, H–C(7)); 4.30–3.30 (*m*, 5 H, CH<sub>2</sub>O, pyr.); 2.1–1.9 (*m*, 4 H, pyr.); 1.48 (s, *t*-Bu). EI-MS: 460 (34, M<sup>+</sup>, C<sub>23</sub>H<sub>28</sub>N<sub>2</sub>O<sub>8</sub><sup>+</sup>).

*tert-Butyl (2S)-2-[[ (1,2,3,4,5,10-hexahydro-1,4,10-trioxopyridazino[4,5-b]quinolin-8-yl)oxy]methyl]pyrrolidine-1-carboxylate (D)*. From *C* (2.3 mmol): *D* (0.84 g, 85%). Yellow solid. <sup>1</sup>H-NMR (500 MHz, (D<sub>6</sub>)DMSO): 13.25, 12.70, 12.28 (3 br. s, 3 NH); 8.11 (d, <sup>3</sup>J = 8.9, H–C(6)); 7.63, 7.61 (*dd'*, H–C(7), H–C(9)); 4.19, 4.09 (*2m*, CH<sub>2</sub>O, CHN (pyr.)); 3.28 (*m*, CH<sub>2</sub>N (pyr.)); 2.05–1.75 (*m*, 2 CH<sub>2</sub> (pyr.)); 1.40 (s, *t*-Bu). EI-MS: 428 (25, M<sup>+</sup>, C<sub>21</sub>H<sub>24</sub>N<sub>4</sub>O<sub>7</sub><sup>+</sup>; 245 (78, [M – CH<sub>2</sub> – pyr. – Boc] + 1)<sup>+</sup>).

*Deprotection of D*: **6**. To a suspension of the above obtained Boc-protected *D* (429 mg, 1.0 mmol) in DMF (15 ml), 32% HCl soln. (2 ml) was added. The mixture was heated to 100° thus resulting in a clear soln. which was stirred for another hour at 100°. After cooling to 20°, H<sub>2</sub>O (150 ml) was added, and the soln. was neutralized with NaHCO<sub>3</sub> (2.5 g, 30 mmol). Stirring was continued for 10 min, the resulting precipitate filtered, thoroughly washed with H<sub>2</sub>O, and dried *in vacuo*: **6** (285 mg, 87%). Light-yellow solid. <sup>1</sup>H-NMR (500 MHz, (D<sub>6</sub>)DMSO): 11.40 (br. s, NH); 7.85 (d, <sup>3</sup>J = 8.7, H–C(6)); 7.56 (br. s, H–C(9)); 7.33 (d, <sup>3</sup>J = 8.0, H–C(7)); 4.25, 4.17, 3.87, 3.20 (*4m*, 5 H, CH<sub>2</sub>O, pyr.); 2.11, 1.98, 1.89, 1.78 (*4m*, 4 H, pyr.). <sup>13</sup>C-NMR (125.7 MHz, (D<sub>6</sub>)DMSO): 175.53 (C(10)); 159.52, 157.01, 154.80 (C(1), C(4), C(8)); 143.92, 142.65 (C(5a), C(4a)); 128.46 (C(9a)); 125.90, 123.75 (C(6), C(9)); 105.41, 103.93 (C(10a), C(7)); 68.54 (CH<sub>2</sub>O); 58.20 (CHN); 46.04 (CH<sub>2</sub>N); 27.35, 24.28 (2 CH<sub>2</sub>). EI-MS: 328 (7, M<sup>+</sup>, C<sub>16</sub>H<sub>16</sub>N<sub>4</sub>O<sub>4</sub><sup>+</sup>); 245 (100, [M – CH<sub>2</sub> – pyr. + 1]<sup>+</sup>).

*2,3-Dihydropyridazino[4,5-b]quinoxaline-1,4-dione (8)*. Diethyl quinoxaline-2,3-dicarboxylate (274 mg, 1.0 mmol; obtained by esterification of quinoxaline-dicarboxylic acid [27]) and 85% hydrazine hydrate (0.5 g, 15.6 mmol) in EtOH (15 ml) were refluxed for 6 h. The resulting precipitate was filtered and washed with 2N HCl, followed by H<sub>2</sub>O: **8** (170 mg, 79%). Yellow solid. <sup>1</sup>H-NMR (400 MHz, (D<sub>6</sub>)DMSO): 11.80 (br. s, 2 NH); 8.38 (non-resolved *AA'* of *AA'BB'*, H–C(6), H–C(9)); 8.13 (unresolved *BB'* of *AA'BB'*, H–C(7), H–C(8)). EI-MS: 214 (100, M<sup>+</sup>, C<sub>10</sub>H<sub>6</sub>N<sub>4</sub>O<sub>2</sub><sup>+</sup>).

*8.3. 2-Amino-7-(thiomethyl)pteridin-4(3H)-ones 10–12 and 14. General Procedure*. To a soln. of sodium ethanolate (5.0 mmoles) in abs. EtOH, freshly prepared from Na (115 mg, 5.0 mmol) in abs. EtOH (15 ml), the appropriate thiol (8.0 mmol) was added and the soln. stirred for 30 min. Then, 2-amino-7-(bromomethyl)pteridin-4(3H)-one hydrobromide (1.0 mmol) [30], prepared from 2-amino-7-methylpteridin-4(3H)-one [29], was



added and the mixture refluxed for 6 h. After adjusting to pH 7, the resulting precipitate was filtered, thoroughly washed with H<sub>2</sub>O and then with acetone, and finally dried.

*2-Amino-7-[(2-aminoethylthio)methyl]pteridin-4(3H)-one (10)*: Only 2 mmol of 2-aminoethanethiol hydrochloride was added: 215 mg (85%) of **10**. Brown solid. <sup>1</sup>H-NMR (500 MHz, DCl in D<sub>2</sub>O): 6.94 (s, H–C(6)); 2.21 (s, CH<sub>2</sub>–C(7)); 1.42 (t, CH<sub>2</sub>N); 1.04 (t, CH<sub>2</sub>S). EI-MS: 252 (0.2, M<sup>+</sup>, C<sub>9</sub>H<sub>12</sub>N<sub>6</sub>OS<sup>+</sup>), 177 (100, [M – H<sub>2</sub>N(CH<sub>2</sub>)<sub>2</sub>S + 1]<sup>+</sup>).

*2-Amino-7-[(propylthio)methyl]pteridin-4(3H)-one (11)*. Yield 225 mg (90%) of **11**. Orange solid. <sup>1</sup>H-NMR (500 MHz, DCl in D<sub>2</sub>O): 6.92 (s, H–C(6)); 2.12 (s, CH<sub>2</sub>–C(7)); 0.62 (t, CH<sub>2</sub>S); –0.38 (sext., CH<sub>2</sub>); –1.04 (s, Me). EI-MS: 251 (1, M<sup>+</sup>, C<sub>10</sub>H<sub>13</sub>N<sub>5</sub>OS<sup>+</sup>), 177 (100, [M – Me(CH<sub>2</sub>)<sub>2</sub>S + 1]<sup>+</sup>).

*2-Amino-7-[(cyclopentylthio)methyl]pteridin-4(3H)-one (12)*. Yield 270 mg (97%) of **12**. Brownish solid. <sup>1</sup>H-NMR (500 MHz, DCl in D<sub>2</sub>O): 6.84 (s, H–C(6)); 2.08 (s, CH<sub>2</sub>–C(7)); 1.11 (q, CHS); –0.08, –0.37, –0.48, –0.59 (4m, 4 CH<sub>2</sub> (cyclopentyl)). EI-MS: 277 (1, M<sup>+</sup>, C<sub>12</sub>H<sub>15</sub>N<sub>5</sub>OS<sup>+</sup>), 177 (100, [M – C<sub>5</sub>H<sub>9</sub>S + 1]<sup>+</sup>).

*2-Amino-7-[(2-thienylthio)methyl]pteridin-4(3H)-one (14)*. Yield 265 mg (91%) of **14**. Brownish solid. <sup>1</sup>H-NMR (500 MHz, DCl in D<sub>2</sub>O): 8.47 (s, H–C(5')); 7.91 (d, <sup>3</sup>J = 5.2, H–C(3')); 7.41 (s, H–C(6)); 7.40 (d, <sup>3</sup>J = 5.2, H–C(4')); 3.03 (s, 1 CH<sub>2</sub>–C(7)); 4.22, 4.14 (2m, 1 H, CH<sub>2</sub>–C(7)). EI-MS: 291 (76, M<sup>+</sup>, C<sub>11</sub>H<sub>9</sub>N<sub>5</sub>OS<sub>2</sub><sup>+</sup>), 177 (100, [M – (C<sub>4</sub>H<sub>3</sub>S)S + 1]<sup>+</sup>).

*2-Amino-7-(ethoxymethyl)pteridin-4(3H)-one (13)*. As described for **10–12** and **14**, without addition of a thiol: 170 mg (77%) of **13**. Brown solid. <sup>1</sup>H-NMR (400 MHz, DCl in D<sub>2</sub>O): 6.88 (s, H–C(6)); 3.00 (s, CH<sub>2</sub>–C(7)); 1.80 (q, MeCH<sub>2</sub>O); –0.70 (t, MeCH<sub>2</sub>O). EI-MS: (221 (1, M<sup>+</sup>, C<sub>9</sub>H<sub>11</sub>N<sub>5</sub>O<sub>2</sub><sup>+</sup>), 177 (100, [M – C<sub>2</sub>H<sub>5</sub>O + 1]<sup>+</sup>).

This work was supported by the *Deutsche Forschungsgemeinschaft* (Grant KL-1204/1).

#### REFERENCES

- [1] K. Kotloff, J. Winickoff, B. Ivanoff, J. Clemens, D. Swerdlow, P. Sansonetti, G. Adak, M. Levine, *Bull. World Health Organiz. (WHO Bull.)* **1999**, *77*, 651.
- [2] W. A. Khan, C. Seas, U. Dhar, M. A. Salam, M. L. Bennish, *Ann. Intern. Med.* **1997**, *1*, 697.
- [3] M. L. Replogle, D. W. Fleming, P. R. Cieslak, *Clin. Infect. Dis.* **2000**, *30*, 515.
- [4] WHO, in 'Overcoming Antimicrobial Resistance', <http://www.who.int/infectious-disease-report/2000/index.html>, 2000.
- [5] J. M. Durand, B. Dagberg, B. E. Uhlin, G. R. Bjork, *Mol. Microbiol.* **2000**, *35*, 924.
- [6] N. Okada, S. Nishimura, *J. Biol. Chem.* **1979**, *254*, 3061.
- [7] J. D. Kittendorf, L. M. Barcomb, S. T. Nonekowsky, G. A. Garcia, *Biochemistry* **2001**, *40*, 14123.
- [8] C. Romier, K. Reuter, D. Suck, R. Ficner, *Biochemistry* **1996**, *35*, 15734.
- [9] B. Frey, J. McCloskey, W. Kersten, H. Kersten, *J. Bacteriol.* **1988**, *170*, 2078.
- [10] R. K. Slany, H. Kersten, *Biochimie* **1994**, *76*, 1178.
- [11] L. Curran, in 'Modification and Editing of RNA', Eds. H. Grosjean and B. Benne, American Society for Microbiology Press, Washington, DC, 1998, p. 493.
- [12] G. R. Björk, in 'tRNA: Structure, Biosynthesis, and Function', Eds. D. Söll and U. L. Rajbhandary, American Society for Microbiology Press, Washington, DC, 1995, p. 165.
- [13] G. Björk, in 'Escherichia coli and Salmonella: Cellular and Molecular Biology', Eds. F. C. Neidhardt, I. R. Curtiss III, J. L. Ingraham, E. C. C. Lin, K. B. Low, B. Magasanik, W. S. Reznikoff, M. Riley, M. Schaechter, H. E. Umbarger, American Society for Microbiology Press, Washington, DC, 1996, p. 861.
- [14] J. M. Durand, N. Okada, T. Tobe, M. Watarai, I. Fukuda, T. Suzuki, N. Nakata, K. Komatsu, M. Yoshikawa, C. Sasakawa, *J. Bacteriol.* **1994**, *176*, 4627.
- [15] C. Romier, K. Reuter, D. Suck, R. Ficner, *EMBO. J.* **1996**, *15*, 2850.
- [16] C. Romier, J. E. Meyer, D. Suck, *FEBS Lett.* **1997**, *416*, 93.
- [17] R. Brenk, L. Naerum, U. Grädler, H.-D. Gerber, G. A. Garcia, K. Reuter, M. T. Stubbs, G. Klebe, *J. Med. Chem.* **2003**, *46*, 1133.
- [18] E. A. Meyer, R. Brenk, R. K. Castellano, M. Furler, G. Klebe, F. Diederich, *ChemBioChem* **2002**, *3*, 250.
- [19] J. K. Luo, R. N. Castle, *J. Heterocycl. Chem.* **1991**, *28*, 205.
- [20] P. R. Gerber, K. Müller, *J. Comput. Aided Mol. Des.* **1995**, *9*, 251.
- [21] 'SYBYL Molecular Modeling Software', 6.8 edn., Tripos, Inc., St. Louis, MO.
- [22] D. D. Perrin 'Dissociation Constants of Organic Bases in Aqueous Solution', Butterworths, London, 1965.
- [23] H. J. Böhm, G. Klebe, *Angew. Chem., Int. Ed.* **1996**, *35*, 2588.

- [24] A. Davis, S. Teague, *Angew. Chem., Int. Ed.* **1999**, *38*, 736.  
[25] H. Gohlke, G. Klebe, *Angew. Chem., Int. Ed.* **2002**, *41*, 2644.  
[26] G. Klebe, T. Mietzner, *J. Comput. Aided Mol. Des.* **1994**, *8*, 583.  
[27] F. D. Chattaway, W. S. Humphrey, *J. Chem. Soc.* **1929**, 645.  
[28] J. H. Mowat, J. H. Boothe, B. L. Hutchings, E. L. R. Stokstad, C. W. Waller, R. B. Angier, J. Semb, D. B. Cosulich, Y. SubbaRow, *J. Am. Chem. Soc.* **1948**, *70*, 14.  
[29] C. B. Storm, R. Shiman, S. Kaufman, *J. Org. Chem.* **1971**, *36*, 3925.  
[30] C. W. Waller, M. J. Fahrenbach, J. H. Boothe, R. B. Angier, B. L. Hutchings, J. H. Mowat, P. J. F. Poletto, J. Semb, *J. Am. Chem. Soc.* **1952**, *74*, 5405.  
[31] G. Fröhlich, P. Kotsonis, H. Traub, S. Taghavi-Moghadam, N. Al-Masoudi, H. Hofmann, H. Strobel, H. Matter, W. Pfeleiderer, H. H. Schmidt, *J. Med. Chem.* **1999**, *42*, 4108.  
[32] 'Selector', Tripos Inc., St. Louis, MO 63144, 1996.  
[33] M. Rarey, B. Kramer, T. Lengauer, G. Klebe, *J. Mol. Biol.* **1996**, *261*, 470.  
[34] U. Grädler, H. D. Gerber, D. M. Goodenough-Lashua, G. A. Garcia, R. Ficner, K. Reuter, M. T. Stubbs, G. Klebe, *J. Mol. Biol.* **2001**, *306*, 455.  
[35] J. Kittendorf, T. Sgraja, G. Klebe, K. Reuter, G. A. Garcia, *J. Biol. Chem.*, submitted.  
[36] H. Gohlke, M. Hendlich, G. Klebe, *Persp. Drug Discov. Design* **2000**, *20*, 115.  
[37] H. Gohlke, M. Hendlich, G. Klebe, *J. Mol. Biol.* **2000**, *295*, 337.  
[38] H. Biere, W. Seelen, *Liebigs Ann. Chem.* **1976**, 1972.  
[39] W. Szeja, *Synthesis* **1979**, 822.

Received February 10, 2003